INTERNATIONAL SYMPOSIUM on MUSICAL and ROOM ACOUSTICS
ISMRA 2016
September 11-13, 2016
La Plata, Buenos Aires, Argentina

Physics of Musical Instruments And the Voice:
Paper ISMRA2016-27

Coupling of a one-dimensional acoustic tube to a three-dimensional acoustic space using finite-difference time-domain methods

R Harrison[(a)], S Bilbao[(b)]

[(a)]Acoustics and Audio Group, The University of Edinburgh, United Kingdom, r.l.harrison-3@sms.ed.ac.uk
[(b)]Acoustics and Audio Group, The University of Edinburgh, United Kingdom, s.bilbao@ed.ac.uk

Abstract

In this paper a simple coupling mechanism between a one-dimensional acoustic tube and a three-dimensional acoustic space is proposed to model the radiation behavior of an open tube. This mechanism is derived from energy conserving principles: the energy leaving the acoustic tube is equal to the energy injected into the acoustic space, and vice versa. The tube-room system is modeled using finite-difference time-domain methods for a box terminated using absorbing boundary conditions. Input impedances are calculated and compared against a frequency domain model terminated using the classic Levine and Schwinger radiation impedance.

Keywords: radiation, FDTD

INTERNATIONAL SYMPOSIUM on MUSICAL and ROOM ACOUSTICS
ISMRA 2016
September 11-13, 2016
La Plata, Buenos Aires, Argentina

Coupling of a one-dimensional acoustic tube to a three-dimensional acoustic space using finite-difference time-domain methods

1 Introduction

The dynamics of an acoustic tube are affected not only by how waves travel within the tube, but also by how the tube interacts with the space it is in. The interaction of the tube and acoustic space can be described by a radiation impedance, given as the ratio of acoustic pressure to volume velocity at the end of the tube. The radiation impedance can then be used as a boundary condition in the wave propagation model. The simplest boundary condition for an open tube is where the pressure at the end of the tube is zero (the radiation impedance is zero) and the wave is completely reflected [1]. This condition sets the resonances of the tube to correspond exactly to its length. In reality this is far too simple a description. Upon reflection, some of the wave energy is transferred into the acoustic space and the effective length of the tube is changed; these are both frequency dependent and are determined by the tube radius.

Multiple radiation models exist for different wavefront shapes. A well documented planar wave model was proposed by Levine and Schwinger [2], which matched a planar wave travelling from a cylinder with a spherical free field. The exact form of this model is difficult to implement in the time domain, so approximations, such as those presented by Caussé *et al.* [3] and Silva *et al.* [4], are useful to use. Bilbao and Chick [5] implemented one of the radiation models in [4] in a finite-difference time-domain (FDTD) model of brass instruments.

Spherical radiation models also exist. Caussé *et al.* [3] suggested scaling the planar radiation impedance by using the ratio of the spherical wavefront area to the planar wavefront area. Hélie and Rodet [6] derived an analytical model by assuming the source for radiation was part of a pulsating sphere. They also provided approximations for efficient use in modelling. Hélie *et al.* [7] tested different radiation models by comparing impedance calculations with measurements from a trombone horn and found that the spherical models performed better, although the actual shape of the radiating wavefront is still unknown. These radiation models perform well when compared to experimentally measured impedances, however, additional models are required to simulate the sound outside of the instrument.

An alternative to using an analytical model is to directly simulate all, or part of, the acoustic field. This means that assumptions about the shape of wavefront are no longer required. Noreland [8] used the combination of the Transmission Matrix Method (TMM) and a two-dimensional FDTD solver to model a brass instrument. In the bell section of the instrument, the acoustic field was solved using FDTD methods in a curvilinear coordinate system to calculate a radiation impedance. The TMM was used for the slowly varying parts of the instrument bore and was terminated with the simulated radiation impedance. Although this method allows for curved wavefronts and mode conversion, there is an issue with increasing numerical dispersion as waves travel into larger cells. This is not an issue for calculating impedances, as the dispersed waves disappear when they reach the absorbing boundary conditions, but will be audible if the

sound in the acoustic field is used as an output. Allen and Raghuvanshi [9] modelled the entire instrument in two-dimensions using a cartesian FDTD method. Unlike [8], the dispersion in this method is constant throughout the domain. However, it is more difficult to include losses, such as viscous and thermal damping at the tube walls, in two-dimensions rather than one.

A combination of one, two and three-dimensional systems has been used to model percussion instruments in the time domain using only FDTD methods [10]. A simple drum is a two-dimensional membrane coupled to a three-dimensional air box; this can be extended to model a snare drum by also coupling the membrane to a one-dimensional string. The coupling conditions between each system are derived from energy conserving principles.

The work presented here follows on from the percussion systems—propagation within the acoustic tube is dealt using a one-dimensional model which is coupled to the three-dimensional acoustic field. The coupling is arrived at through energy conserving principles. For simplicity, only lossless wave propagation is considered, but losses can be easily implemented [5]. The continuos domain model is presented in Section 2, which includes wave propagation in one and three dimensions, the absorbing boundary conditions used to terminate the acoustic field and the coupling between the tube and acoustic field. The model is then discretised in Section 3 where FDTD operators are introduced along with discrete energy calculations which are used to couple the tube and the acoustic field. Results using this scheme are presented in Section 4 and concluding remarks are made in Section 5.

2 Model

Here lossless wave propagation is considered within the acoustic tube and acoustic field.

2.1 Acoustic tube and three-dimensional wave equations

The dynamics of a lossless, linear, acoustic tube can be described by the horn equation in first order form

$$\frac{S}{\rho c^2}\partial_t p = -\partial_z (Sv), \quad \rho \partial_t v = -\partial_z p, \quad z \in [0, L_1] \tag{1}$$

where $p(z,t)$ and $v(z,t)$ are the acoustic pressure and particle velocity at axial position z and time t, $S(z)$ is the cross-sectional area of the acoustic tube, ρ and c are the density of air and speed of sound, L_1 is the length of the acoustic tube and ∂_x and ∂_t are partial derivatives with respect to position and time.

The dynamics of air in a cubic box can be described by the second order form of the three-dimensional wave equation. In Cartesian coordinates this is

$$\partial_{tt}\Psi = c^2 (\partial_{xx} + \partial_{yy} + \partial_{zz})\Psi, \quad x, y, z \in [0, L_3] \tag{2}$$

where $\Psi(\mathbf{x},t)$ is the acoustic velocity potential at coordinate $\mathbf{x} = [x, y, z]$ and L_3 is the side length of the box. The pressure, $p_{3D}(\mathbf{x},t)$ and particle velocity $\mathbf{v}_{3D}(\mathbf{x},t)$, in three dimensions are given by

$$p_{3D} = \rho \partial_t \Psi, \quad \mathbf{v}_{3D} = -\nabla \Psi \tag{3}$$

where ∇ is the gradient operator.

2.2 Absorbing boundary conditions

Absorbing boundary conditions of the first-order Engquist-Majda type are applied to the walls of the box [11]

$$\frac{1}{c}\partial_t \Psi + \mathbf{n}\cdot\nabla\Psi = 0, \quad \mathbf{x}\in\partial\mathscr{V} \tag{4}$$

where $\partial\mathscr{V}$ denotes the boundary of the box.

2.3 Coupling of systems

The acoustic tube and three-dimensional box are coupled by a surface, Ω, within the box that is perpendicular to the z axis and allows energy to transfer between the end of the instrument and the box, and vice-versa—see Figure 1.

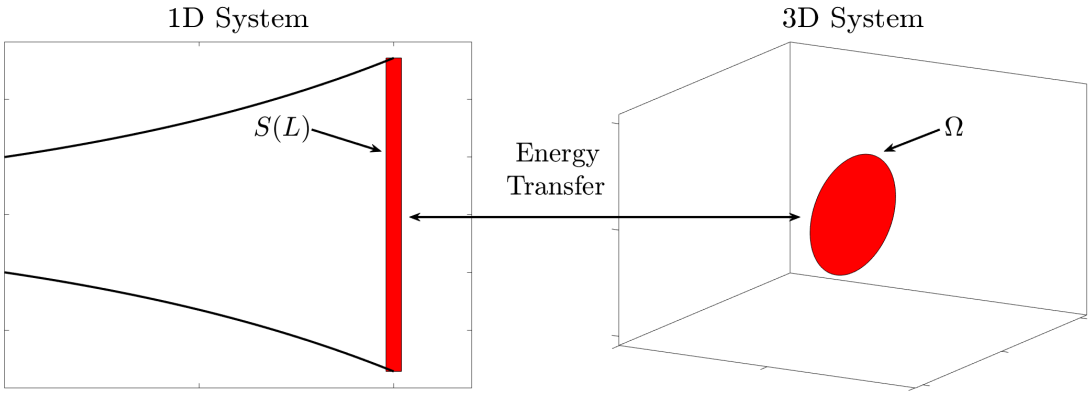

Figure 1: Left: end of acoustic tube. Right: acoustic field with surface, Ω, that allows for energy transfer between the tube and the box.

The evolution of the energy in the acoustic tube, $\mathscr{H}_{tube}$, and box, $\mathscr{H}_{box}$, is

$$\partial_t \mathscr{H}_{tube} = -|pSv|_0^L, \quad \partial_t \mathscr{H}_{box} = -\mathscr{B}_{walls} - \int_\Omega \rho\,\partial_t\Psi\partial_z\Psi dS \tag{5}$$

where $\mathscr{B}_{walls}$ denotes energy lost at the box boundaries. In the acoustic tube, energy loss at the end of the tube is energy put into the box on the surface Ω, and vice versa, so that

$$pSv|_L = -\int_\Omega \rho\,\partial_t\Psi\partial_z\Psi dS \tag{6}$$

3 Numerical method

Discrete operators are introduced here along with the discrete energy analysis required to couple the acoustic tube and acoustic field. Discretisation of the absorbing boundary conditions

are omitted but can be found in [10] and the identities used in the energy analysis can be found in [12].

3.1 Grids and finite-difference operators

To model wave propagation in the acoustic tube, two interleaved grids are used to sample the pressure and velocity fields so that $p(lh_1, nk) = p_l^n$ and $v((l+\frac{1}{2})h_1, (n+\frac{1}{2})k) = v_{l+\frac{1}{2}}^{n+\frac{1}{2}}$, where l and n are integers that label points in space and time, and h_1 and k denote spacings on the spatial and temporal grids. The velocity potential is sampled so that $\Psi(\mathbf{l}h_3, (n+\frac{1}{2})k) = \Psi_{\mathbf{l}}^{n+\frac{1}{2}}$, where $\mathbf{l} = [l_x, l_y, l_z]$ and l_x, l_y and l_z are integers that label the x, y and z coordinates. h_3 is the grid spacing for the air box.

Discrete operators that approximate the continuous differential operators can be defined in terms of temporal and spatial shifting operators $e_{t\pm}$, $e_{x\pm}$, $e_{y\pm}$ and $e_{z\pm}$, the action of which is

$$e_{t\pm}p_l^n = p_l^{n\pm1}, \quad e_{z\pm1}p_l^n = p_{l\pm1}^n, \quad e_{z\pm1}\Psi_{l_x,l_y,l_z}^{n+\frac{1}{2}} = \Psi_{l_x,l_y,l_z\pm1}^{n+\frac{1}{2}}, \tag{7}$$

Similarly for $e_{x\pm}$ and $e_{y\pm}$. Discrete approximations to difference operators are

$$\partial_t \approx \delta_{t\pm} = \pm\frac{e_{t\pm}\pm1}{k}, \quad \partial_t \approx \delta_{t\cdot} = \frac{e_{t+}-e_{t-}}{2k}, \quad \partial_{tt} \approx \delta_{tt} = \delta_{t+}\delta_{t-} \tag{8a}$$

$$\partial_z \approx \delta_{z\pm} = \pm\frac{e_{z\pm}\pm1}{h}, \quad \partial_{zz} \approx \delta_{zz} = \delta_{z+}\delta_{z-} \tag{8b}$$

and likewise for derivatives with respect to x and y. Note that $\delta_{z\pm}$ differs whether it is used in one or three dimensions, as a different length step is required.

The following averaging operators are used to centre schemes

$$\mu_{t\pm} = \frac{e_{t\pm}+1}{2}, \quad \mu_{z\pm} = \frac{e_{z\pm}+1}{2} \tag{9}$$

One dimensional inner products are

$$<f,g>=\sum_{l=0}^{N} h_1 f_l^n g_l^n, \quad <f,g>'=\sum_{l=1}^{N-1} h_1 f_l^n g_l^n + \frac{h_1}{2}f_0^n g_0^n + \frac{h_1}{2}f_N^n g_N^n \tag{10}$$

and norms

$$<f,f>' = ||f||'^2, \quad <f,f> = ||f||^2 \tag{11}$$

The one-dimensional inner products can be easily extended to three dimensions by using three summations.

3.2 Finite-difference scheme

Applying operators from the previous section to (1) and (2) gives

$$\frac{\bar{S}_l}{\rho c^2}\delta_{t+}p_l^n = -\delta_{x-}\left(S_{l+\frac{1}{2}}v_{l+\frac{1}{2}}^{n+\frac{1}{2}}\right), \quad \rho\,\delta_{t-}v_{l+\frac{1}{2}}^{n+\frac{1}{2}} = -\delta_{x+}p_l^n, \quad l\in[0,N_1] \tag{12a}$$

$$\delta_{tt}\Psi_{\mathbf{l}}^{n+\frac{1}{2}} = c^2\delta_{\nabla}\Psi_{\mathbf{l}}^{n+\frac{1}{2}}, \quad l_x, l_y, l_z \in [0, N_3] \tag{12b}$$

where $\bar{S}_l = \mu_{z-}S_{l+\frac{1}{2}}$, $\delta_{\nabla} = \delta_{xx} + \delta_{yy} + \delta_{zz}$ is the discrete Laplacian, $N_1 = \text{floor}(\text{L}_1/\text{h}_1)$ and $N_3 = \text{floor}(\text{L}_3/\text{h}_3)$. For implementation and manipulation in the next section, Ψ is decomposed into a vector of length N_3^3, see Appendix of [13] .

3.3 Discrete energy and coupling

Taking the inner product of (12a) with $\mu_{t+}p_l$ and using summation by parts gives

$$\delta_{t+}\mathfrak{h}_{tube} = \mu_{t+}p_0\mu_{x-}\left(S_{\frac{1}{2}}v_{\frac{1}{2}}\right) - \mu_{t+}p_N\mu_{x-}\left(S_{N+\frac{1}{2}}v_{N+\frac{1}{2}}\right) \tag{13}$$

where $\mathfrak{h}_{tube} = \frac{1}{2\rho c^2}||\sqrt{\bar{S}}p||'^2 + \frac{\rho}{2} < Sv, e_{t-}v >$ is the stored energy in the tube and temporal indices have been suppressed. The right hand side of (13) gives the power change at the input and output of the tube.

To get the discrete energy of the box, the inner product of (12b) is taken with $\frac{\rho}{c}\delta_{t\cdot}\Psi_{\mathbf{l}}$ which, after using summation by parts, gives

$$\delta_{t+}\mathfrak{h}_{box} = -\rho\sum_{\mathbf{l}\in\Omega} h_3^2\delta_{t\cdot}\Psi_{\mathbf{l}}\delta_{z-}\Psi_{\mathbf{l}} - \mathfrak{b}_{walls} \tag{14}$$

where $\mathfrak{h}_{box} = \frac{\rho}{2c^2}||\delta_{t-}\Psi||^2 + 0.5\rho\left(< \delta_{x-}\Psi, e_{t-}\delta_{x-}\Psi > + < \delta_{y-}\Psi, e_{t-}\delta_{y-}\Psi > + < \delta_{z-}\Psi, e_{t-}\delta_{z-}\Psi >_{\bar{\Omega}}\right)$ and $\bar{\Omega}$ denotes that the inner product is not taken on the surface Ω. $\mathfrak{b}_{walls}$ denotes the power loss at the walls due to the absorbing boundary conditions (the expression for this is omitted for brevity).

On Ω the spatial derivative has been rewritten as $\delta_{zz} = \frac{1}{h_3}(\delta_{z+} - \delta_{z-})$. This allows for a directional energy sink/source in the room—only energy in front of the surface is allowed to be transferred into the acoustic tube.

The summation in (14) can be considered as a vector multiplication of the elements that lie on omega. Using the same argument as for (6)

$$-\rho h_3^2\delta_{t\cdot}\Psi_{\Omega}^T\delta_{z-}\Psi_{\Omega} = \mu_{t+}p_N\mu_{x-}\left(S_{N+\frac{1}{2}}v_{N+\frac{1}{2}}\right) \tag{15}$$

where ^{T} denotes the transpose and Ψ_{Ω} is a vector of entries lying on the bell plane. Defining a vector $\mathbf{q}$ of size $N_{\Omega}\times 1$, where N_{Ω} is the number of elements on the surface Ω, whose elements are 1 at the entries that correspond to points on the surface Ω leads to

$$\rho\,\delta_{t\cdot}\Psi_{\Omega} = \mathbf{q}\mu_{t+}p_N \tag{16}$$

This then gives from (15)

$$-h_3^2\mathbf{q}^T\delta_{z-}\Psi_{\Omega} = \mu_{x-}\left(S_{N+\frac{1}{2}}v_{N+\frac{1}{2}}\right) \tag{17}$$

Equations (16) and (17) can be used to get an update of the pressure and velocity at the end of the acoustic tube. The first of (12a) can be rewritten as

$$\frac{2\bar{S}}{\rho c^2 k}\left(\mu_{t+} - 1\right)p_N = -\frac{2}{h_1}\left(\mu_{x-} - e_{x-}\right)S_{l+\frac{1}{2}}v_{l+\frac{1}{2}} \tag{18}$$

On Ω, (12b) can be rewritten as

$$\frac{2\rho}{c^2 k}\left(\delta_{t\cdot} - \delta_{t-}\right)\Psi_{\mathbf{l}} + \frac{\rho}{h_3}\delta_{z-}\Psi_{\mathbf{l}} = \rho\,\delta_{xx}\Psi_{\mathbf{l}} + \rho\,\delta_{yy}\Psi_{\mathbf{l}} + \frac{\rho}{h_3}\delta_{z+}\Psi_{\mathbf{l}} \tag{19}$$

Using (16), multiplying by $\mathbf{q}^T$ and substituting (17) leads to the following linear system when combined with (18)

$$\mathbf{A}\mathbf{y} = \mathbf{B} \tag{20}$$

where

$$\mathbf{A} = \begin{bmatrix} \frac{2\bar{S}_N}{\rho c^2 k} & \frac{2}{h_1} \\ \frac{2N_\Omega}{c^2 k} & -\frac{\rho}{h_3^3} \end{bmatrix}, \quad \mathbf{y} = \begin{bmatrix} \mu_{t+} p_N^n \\ \mu_{x-}\left(S_{N+\frac{1}{2}} v_{N+\frac{1}{2}}^{n+\frac{1}{2}}\right) \end{bmatrix} \tag{21a}$$

$$\mathbf{B} = \begin{bmatrix} \frac{2\bar{S}_N}{\rho c^2 k} p_N^n + \frac{2}{h_1} S_{N-\frac{1}{2}} v_{N-\frac{1}{2}}^{n+\frac{1}{2}} \\ \rho \mathbf{q}^T \left(\frac{2}{c^2 k}\delta_{t-} + \delta_{xx} + \delta_{yy} + \frac{1}{h_3}\delta_{z+}\right)\Psi_\Omega^{n+\frac{1}{2}} \end{bmatrix} \tag{21b}$$

4 Results

Simulations were performed for a cylindrical tube of length 1 m and radius 0.05 m in a cubic box of side length 0.5 m using the coupling condition in Section 3. The acoustic tube was excited using a volume velocity source, as in [5]. Figure 2 shows the system excited with a 10 sample long Hann pulse.

The input impedance can be calculated by exciting the system with a volume velocity whose first sample is a 1 and the rest are 0 and then taking the Fourier transform of the backwards time averaged pressure at $l = 0$ (so that both the pressure and volume velocity are correctly aligned). These results were compared with the exact solution using the radiation condition given by Levine and Schwinger [2]. The sample rate was 50 kHz and the simulation time was 10 s. The Courant condition was set to $ck/h_1 = 0.99$ and $ck/h_3 = 0.99/\sqrt{3}$. The bell plane was positioned in the centre of the box and aligned with the z axis. Points on the bell plane were chosen so that they lay within the tube radius, see Left of Figure 3. The ratio of the area of the bell plane, $N_\Omega h_3^2$, to the actual area is 0.9279. A staircased cylindrical wall was set behind the bell plane also by setting the spatial derivatives to zero. At right of Figure 3 shows the input impedance using the Levine and Schwinger radiation model and that calculated using the FDTD scheme.

The position and magnitude of the first five input impedance peaks were calculated using a quadratic fitting procedure and presented in Table 1. The positions of the input impedance peaks from the simulated model are 1% different from those calculated by the exact model. The magnitude of the peaks are significantly different, ranging from 5% to 70%. For frequencies up to 600Hz, the reflection function calculated from Levine and Schwinger's model has a value greater than 0.9, meaning that the the system is almost lossless in this frequency range and waves are almost entirely reflected. For the lowest peak, it would be reasonable to suggest

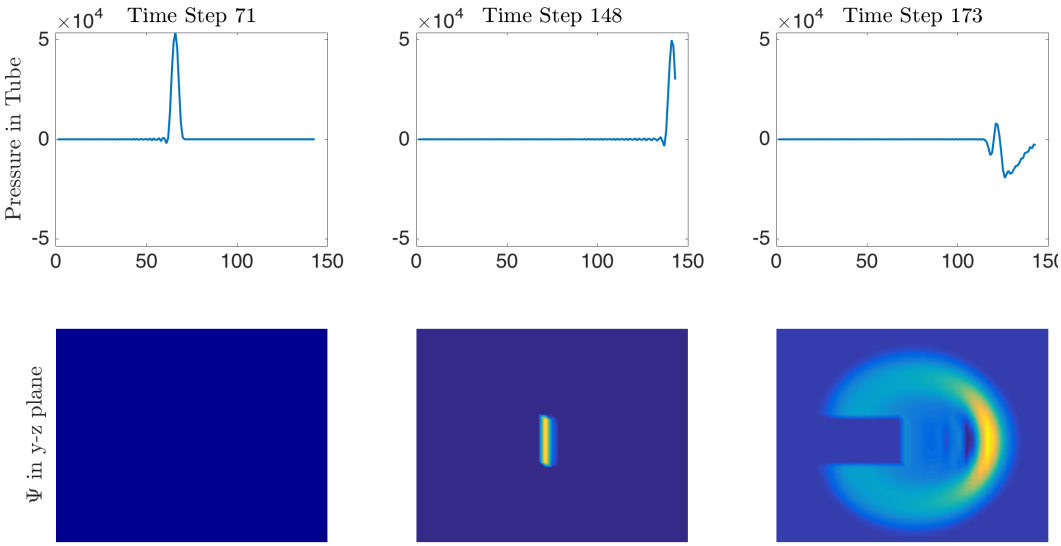

Figure 2: Wave propagation within the tube (top) and box (bottom) when the tube is excited with a 10 sample long Hann pulse volume velocity. Left: pulse halfway through tube. Middle: pulse reaches boundary between tube and box. Right: pulse has partially reflected at the end of the tube and travelling back to entrance, rest of pulse is in the box.

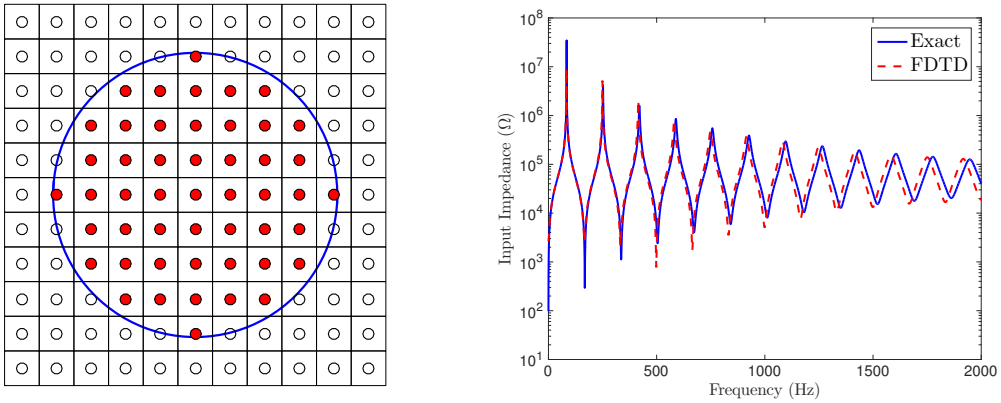

Figure 3: Left: Staircase approximation of bell on Ω. Blue circle is actual radius, empty dots are points not lying in circle, red dots are in circle. Right: Input impedances of a cylinder calculated using the analytical solution with the Levine and Schwinger radiation condition (blue) and using the FDTD coupled system (dashed red).

that it's magnitude would be close to infinity, which would be difficult to match with a fitting procedure.

Figure 4 plots the normalised summed energy of the system, showing discrete changes in the energy due to machine precision [10]. There is a larger jump in energy around the 170^{th} time

Peak Number	1	2	3	4	5
Exact Frequency (Hz)	83.99	252.01	420.25	588.75	757.53
FDTD Frequency (Hz)	83.21	249.50	415.35	581.23	748.54
Frequency Difference (%)	0.92	1.00	1.16	1.28	1.19
Exact Magnitude (MΩ)	30.34	4.22	1.59	0.86	0.54
FDTD Magnitude (MΩ)	9.06	5.18	2.09	0.81	0.48
Magnitude Difference (%)	70.14	22.73	31.44	5.33	13.02

Table 1: Impedance peak positions and magnitudes for simulations in Figure 3

step when the wave passes from the tube to the room — this jump is due to different step sizes in the two systems.

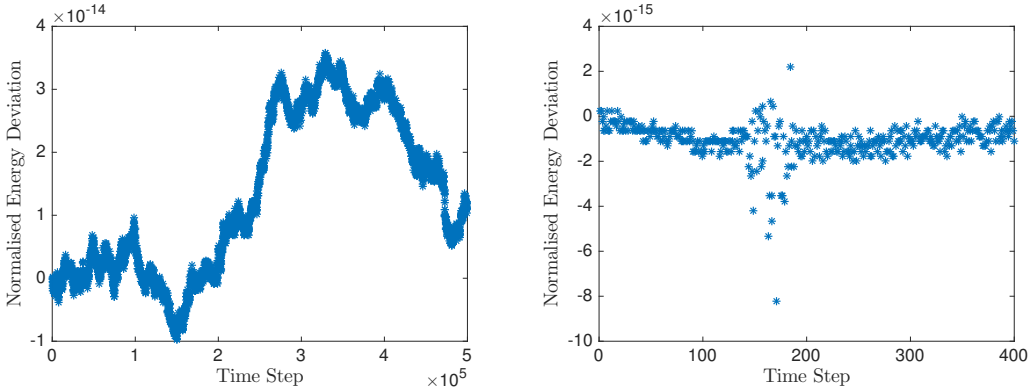

Figure 4: Left: Energy deviation over simulation (note this has been sampled to show every 100^{th} sample). Right: Snapshot of the energy variation of the simulation for the first 400 samples.

5 Conclusions and Future Work

The model presented in this paper is a reasonable method for modelling sound radiation from an acoustic tube. The current staircasing method of choosing the bell plane can be improved by using fitted cells which would better approximate the area of the bell plane. For flaring tubes, such as brass instruments, a larger portion of the bell could be modelled (as in [8]) to accommodate the change of wave shape and transfer of energy between modes. The box model could also be enlarged so that the instrument was playing in a performance space. This would dramatically increase the computation time, however, and further optimisation of the simulation using Graphics Processing Units would be needed to improve performance.

Acknowledgements

This work was supported by the European Research Council under grant number ERC-2011-StG-279068-NESS.

References

[1] N. H. Fletcher and T. D. Rossing, *The Physics of Musical Instruments, Second Edition*. Springer, 1998.

[2] H. Levine and J. Schwinger, "On the radiation of sound from an unflanged circular pipe," *Physical Review*, vol. 73, no. 4, pp. 383–406, 1948.

[3] R. Caussé, J. Kergomard, and X. Lurton, "Input impedance of brass musical instruments - comparison between experiment and numerical models," *Journal of the Acoustical Society of America*, vol. 75, no. 1, pp. 241–254, 1984.

[4] F. Silva, P. Guillemain, J. Kergomard, B. Mallaroni, and A. N. Norris, "Approximation formulae for the acoustic radiation impedance of a cylindrical pipe," *Journal of Sound and Vibration*, vol. 322, pp. 255–263, 2009.

[5] S. Bilbao and J. Chick, "Finite difference time domain simulation for the brass instrument bore," *Journal of the Acoustical Society of America*, vol. 134, no. 5, pp. 3860–3871, 2013.

[6] T. Hélie and X. Rodet, "Radiation of a pulsating portion of a sphere: Application to horn radiation," *Acta Acustica united with Acustica*, vol. 89, pp. 565–577, 2003.

[7] T. Hélie, T. Hézard, R. Mignot, and D. Matignon, "One-dimensional acoustic models of horns and comparison with measurements," *Acta Acustica united with Acustica*, vol. 99, pp. 960–974, 2013.

[8] D. Noreland, "A numerical method for acoustic waves in horns," *Acta Acustica united with Acustica*, vol. 88, pp. 576–586, 2002.

[9] A. Allen and N. Raghuvanshi, "Aerophones in flatland: Interactive wave simulation of wind instruments," *ACM Trans. Graph.*, vol. 34, pp. 134:1–134:11, July 2015.

[10] A. Torin, *Percussion Instrument Modelling in 3D: Sound Synthesis Through Time Domain Numerical Simulation*. PhD thesis, The University of Edinburgh, 2015.

[11] B. Engquist and A. Majda, "Absorbing boundary conditions for the numerical simulation of waves," *Mathematics of Computation*, vol. 31, no. 139, pp. 629–651, 1977.

[12] S. Bilbao, *Numerical Sound Synthesis: Finite Difference Schemes and Simulation in Musical Acoustics*. Wiley, 2009.

[13] B. Hamilton, S. Bilbao, and C. J. Webb, "Revisiting implicit finite difference schemes for 3-d room acoustics simulations on gpu," in *Proc. of the* 17^{th} *Int. Conference on Digital Audio Effects*, (Erlangen, Germany), September 2014.